

Experimental Investigations on the Adsorptive Behavior of H₂O Vapor on HTC Char Particles[#]

Tim Eisenbach^{1*}, Horacio A. Duarte², Carsten Wedler³, Christin Pflieger⁴, Martin Muhler⁴, Roland Span¹

¹ Thermodynamics, Ruhr University Bochum, 44801 Bochum, Germany

² Department of Chemical and Natural Gas Engineering, Texas A&M University Kingsville, 955 N University Blvd, Kingsville, TX 78363, US

³ Department of Chemical Engineering, Imperial College London, London, SW7 2AZ, UK

⁴ Laboratory of Industrial Chemistry, Ruhr University Bochum, 44801 Bochum, Germany

ABSTRACT

In gasification and combustion processes of biomass, the adsorptive mass transport of relevant gases in the porous structure of particles is of most interest, since diffusion can be a limiting factor to the reaction rate during conversion. Therefore, this study presents an experimental data basis for the kinetic adsorption behavior of H₂O vapor as one of the three main components in an oxyfuel atmosphere. Considering the implementation of diffusion and mass transport properties in char conversion modeling, a pore-structure dependent kinetic adsorption (PSK) model was previously developed based on kinetic adsorption measurements. After the successful validation using comprehensive kinetic adsorption data sets of O₂ and CO₂, this work provides new insights into the distinct adsorption behavior of H₂O vapor in order to develop the PSK model even further.

Keywords: Biomass conversion, adsorption kinetics, water-vapor adsorption measurement, temperature-programmed desorption measurements, pore-structure dependent kinetic adsorption model

NOMENCLATURE

Abbreviations

EOS	Equation of state
HTC	Hydrothermal carbonization
IUPAC	International union of pure and applied chemistry
MCC	Microcrystalline cellulose
mi	Micropores
mm	Meso- to macropores
NLDFT	Nonlocal density functional theory
OFG	Oxygen functional groups

PSD	Pore Size Distribution
PSK	Pore-structure dependent kinetic adsorption
TPD	Temperature-programmed desorption
ul	Ultramicropores
VLE	Vapor-liquid-equilibrium
<i>Symbols</i>	
a	Kinetic time constant
A	Surface area
c	Thickness of sorption layer
H	Heat of adsorption
k	Pressure dependence
n	Kinetic temperature dependence
n_s	Specific molar amounts
m_{01}	Lifted mass
m_{ads}	Adsorbed mass
m_s	Sample mass
M	Molecular mass
p	Pressure
p_{sat}	Saturation pressure
q	Adsorbed loading
R	Molar gas constant
t	Time
T	Temperature
T_{ads}	Adsorption temperature
T_{vapor}	Vapor temperature
V_{01}	Lifted Volume
W_{01}	Weighing value
α	Balance calibration factor
ϕ	Coupling factor
ρ	Mass density
ρ_m	Molar density

1. INTRODUCTION

In char conversion modeling, a close investigation of the associated mass transport of relevant gases (CO_2 , O_2 , and H_2O) is important as it can be a limiting factor for solid fuel reactions and gasification rates [1,2]. When considering the gasification of biomass in an oxyfuel atmosphere, mass transport properties differ significantly compared to conventional combustion and gasification processes of solid fossil fuels [2]. The composition of the atmosphere is shifted with respect to higher concentrations of non-inert compounds like CO_2 and H_2O compared to conventional combustion atmospheres and, thus, sorption and diffusion characteristics of oxygen are affected [3]. In order to provide a description of the adsorption and diffusion processes in char conversion modeling, a pore-structure dependent kinetic adsorption (PSK) model was formulated by Wedler and Span [4]. This model takes the influence of solid fuel morphologies in terms of the pore size distribution (PSD) into account. Based on kinetic adsorption measurements, the model was successfully validated for the adsorption of CO_2 [4] and O_2 [5].

In this work, the characteristic of the adsorption system with H_2O is investigated based on kinetic adsorption measurements. Using the same biomass fuel as in [4,5], the measurements are intended as a basis for further developments of the PSK model. The adsorption of the condensable fluid H_2O is generally known for its deviating behavior from classic gas-phase adsorption systems due to the associative character of H_2O [6,7]. Therefore, the most significant particularities of the adsorption system are to be highlighted within this work. The oxygen functional groups (OFG) on carbon surfaces are known to have a strong influence on the adsorption tendency of gaseous agents and especially of H_2O as they act as hydrophilic sites [8]. Considering that, this work also provides a comprehensive temperature-programmed desorption measurement and analysis for the investigated char. Furthermore, the PSD of the solid fuel is considered in this work as it influences the growth and coalescence of adsorbed H_2O clusters and, thus, the pore-filling process.

2. EXPERIMENTAL

2.1 Char synthesis and properties

The adsorption kinetics were investigated for a pulverized char, which was synthesized by hydrothermal carbonization (HTC) of microcrystalline cellulose (MCC) and subsequent slow-heating rate ($5\text{ }^\circ\text{C min}^{-1}$) pyrolysis for 2 h at $800\text{ }^\circ\text{C}$ in flowing N_2 . The detailed procedure was described elsewhere [9,10]. The resulting, ash-free MCC-HTC char, contains only carbon, hydrogen, and

oxygen. Thereby, it is a suitable reference for systematic investigations on pore characteristics in conversion processes and, thus, on sorption and diffusion behavior [11].

2.1.1 Pore surface characterization

Wedler and Span [4] already carried out a comprehensive pore surface analysis of the investigated MCC-HTC char, taking advantage of two-dimensional, nonlocal density functional theory (2D-NLDFT) calculations. This method combines the adsorption isotherms for N_2 and CO_2 in a simultaneous dual gas analysis [12]. From the PSD and the classification of different pore regimes, according to the IUPAC [13], the pore surfaces (see Table 1) can be calculated. Accordingly, the ultramicropores (ul) are defined in the pore diameter range of $d_p < 0.7\text{ nm}$, the micropores (mi) for $0.7\text{ nm} < d_p < 2\text{ nm}$, and the meso-to macropores (mm) for $d_p > 2\text{ nm}$.

Table 1 Pore surface area of the MCC-HTC char

A_{mm} [m^2/g]	39.3
A_{mi} [m^2/g]	225.1
A_{ul} [m^2/g]	286.6

2.1.2 Temperature-programmed desorption measurement and analysis

In order to quantify the amounts of individual OFG on the surface of the investigated MCC-HTC char and, therefore, the impact on the adsorption measurements, a temperature-programmed desorption (TPD) measurement and analysis of the evolving gases were performed. In the measurement, 100 mg of char were heated with 5 K min^{-1} to $800\text{ }^\circ\text{C}$ in 20 ml min^{-1} He. Simultaneously, the effluent gas was analyzed by a multi-channel detector (NGA 2000 MLT4 by Rosemount). The quantified amounts of H_2O , CO_2 , and CO as a function of sample temperature were separated into Gaussian contributions of different decomposing OFG by deconvolution [14]. The assignment of individual OFG to peaks in the three effluent gas curves was realized based on the type of released gas and the relative thermal stability [15].

2.2 Gravimetric sorption measurements

The gravimetric sorption analyzer was first set up in the work of Rösler and Wedler [16] to be able to measure the adsorption of condensable fluids. It is based on a magnetic suspension balance (ISOSORP) of Rubotherm (since 2016 TA Instruments). The balance weighs the sample container with the filled in pulverized sample as well as all connected parts (see Figure 1), contactless and

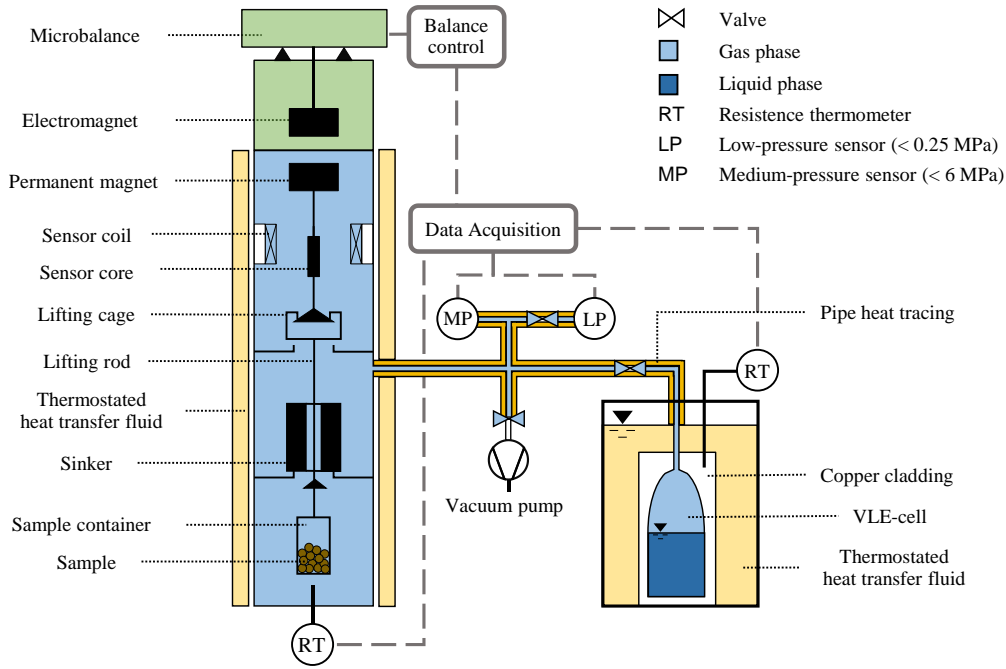


Fig. 1 Gravimetric sorption system for the measurements of adsorption kinetics with condensing fluids, according to Rösler and Wedler [16]

isolated from the physical conditions within the measuring cell. Different measuring positions can be addressed by changing the electromagnetic field in which the permanent magnet is kept levitating.

At zero point (ZP) only the permanent magnet and the sensor core are lifted, while at measuring point 1 (MP1) the lifting cage, lifting rod, and the filled sample container are lifted as well. At measuring point 2 (MP2) all adjustable parts are lifted, including a density sinker. The measuring cell is equipped with a sheathing containing temperature-controlled heat transfer fluid.

A second temperature-controlled cell provides a vapor-liquid-equilibrium (VLE) system of the investigated fluid. The vapor pressure can be set by adjusting the temperature of the heat transfer fluid in a bath thermostat. When opening the valve connecting the VLE-cell with the evacuated measuring cell, the gas-phase is fed into the measuring cell. A pipe heating avoids condensation at the colder pipe walls.

In this work, the adsorption kinetics and equilibria were measured along three isotherms at $T_{\text{ads}} = (25.4, 35.3, 48.8) \text{ } ^\circ\text{C}$. Accordingly, each equilibrium point of the isotherm is related to one time-dependent adsorption kinetic. Each isotherm is obtained from several equilibrium adsorption loadings at different vapor pressures. The vapor pressure, controlled by the temperature T_{vapor} in the VLE-cell, is limited by the adsorption temperature T_{ads} . The equilibrium loadings for one isotherm (see Figure 3) are plotted over $p/p_{\text{sat},t}$,

with p_{sat} representing the saturation pressure of the measurement system, determined by T_{ads} . Before each measurement run, the system is evacuated using a rotary vane vacuum pump. From the evacuated state, the measuring cell is filled with vapor and the weighing value of the balance $W_{01}(p, T_{\text{ads}}, t)$ increases due to the adsorption of H_2O molecules on the surface of the porous particles. During the kinetic adsorption measurement, the balance position is kept in MP1 to obtain a seamless weighing value. After reaching the equilibrium value the balance is set to the auto-position-control (APC), switching the position between MP1 and ZP. Besides the calculation of the equilibrium loadings at this point, the weighing signal $W_1(p, T_{\text{ads}}, t)$ can be corrected with the ZP resulting in $W_{01}(p, T_{\text{ads}}, t)$, which cancels out any balance drifts.

The weighing value has to be converted to the mass of the adsorbed molecules $m_{\text{ads}}(p, T_{\text{ads}}, t)$ according to the mass balance in Eq. (1).

$$m_{\text{ads}}(p, T_{\text{ads}}, t) = \frac{W_{01}(p, T_{\text{ads}}, t)}{\alpha \cdot \phi(\rho_{\text{H}_2\text{O}}, \text{EOS}, t)} - m_{01} + \rho_{\text{H}_2\text{O}, \text{EOS}}(T_{\text{VLE}}, t) \cdot V_{01} \quad (1)$$

The value needs to be corrected by the balance calibration factor α and the contribution of the force transmission error (FTE) ϕ . Furthermore, the mass of all parts lifted additionally to the actual mass of adsorbed molecules, m_{01} , are subtracted. Also, all lifted parts are

affected by the buoyancy depending on the density of the H₂O vapor in the measuring cell $\rho_{\text{H}_2\text{O}, \text{EOS}}(T_{\text{VLE}}, t)$ and the volume of all lifted parts V_{01} . The density was calculated using the equation of state (EOS) by Wagner and Pruss [17]. More information on this procedure and the determination of the FTE value can be found in Rösler and Wedler [16].

From Eq. (1) the time-dependent adsorption loading $q(p, T_{\text{ads}}, t)$ can be derived with the molecular mass of H₂O, $M_{\text{H}_2\text{O}}$, and the mass of the sample m_s .

$$q(p, T_{\text{ads}}, t) = \frac{m_{\text{ads}}(p, T_{\text{ads}}, t)}{M_{\text{H}_2\text{O}} \cdot m_s} \quad (2)$$

3. PSK MODEL

The adsorption measurements performed in this work intend to hold as a data basis for the adjustment and further development of the PSK model. The adsorption loadings as calculated from Eq. (2) are modelled with respect to time, temperature and pressure, according to Eq. (3). The three terms describe and model the adsorption process in different pore regimes (mm, mi, ul), corresponding to the individual pore surface area A_i (see chapter 2.1.1). Each term is divided into a time-independent equilibrium part and a kinetic part. At equilibrium state and for each pore regime i , the parameters of the effective sorption layer thickness c_i , the pressure dependence k_i , and the heat of adsorption H_i are defined with respect to a Langmuir isotherm approach. The kinetic adsorption behavior in each pore is represented with the time constant of the individual pore filling process a_i and the kinetic temperature dependence n_i . Further, the reference temperature T_{ref} is defined as 298.15 K, according to Wedler and Span [4] and the molar density of the adsorbate phase can be considered as the temperature dependent density of the saturated liquid H₂O, $\rho_m(T)$.

$$q(p, T, t) = \rho_m(T) \cdot \sum_{i=1}^3 A_i \cdot c_i \frac{p \cdot k_i \cdot e^{H_i/R \cdot T}}{1 + p \cdot k_i \cdot e^{H_i/R \cdot T}} \cdot \left(1 - e^{-\frac{t}{a_i \left(\frac{T}{T_{\text{ref}}} \right)^{-n_i}}}} \right) \quad (3)$$

4. RESULTS AND FINDINGS

4.1 TPD deconvolution and OFG quantification

The deconvolution results of the different effluent gas curves are shown in Figure 2. Generally, the H₂O signals are broadened and shifted to higher temperatures because of readsorption prior to

detection. The first contribution to evolving H₂O is physisorbed molecules. However, their amount is minor due to the flushing of the sample prior to heating with inert gas. Much larger contributions originate from clusters bound to acid groups and from the condensation of neighboring OFG, most prominently the condensation of two carboxylic acids to *in situ* generated anhydrides, the so-called condensed acids [18]. These OFG are destabilized and decompose directly into CO₂ and CO, prior to the analogous two-step decomposition of anhydrides present in the char prior to the TPD treatment. The CO₂ curve contains an additional contribution between the condensed acids and anhydrides. This contribution is assigned to carboxylic acids, while lactones decompose at higher temperatures. The two most stable types of OFG are phenols/ethers and carbonyls/quinones which decompose under the release of CO in the higher temperature range. The areas of the peak contributions enabled to determine the specific molar amounts of the individual OFG as summarized in Table 2.

Overall, effluent gases detected up to 800 °C account for about 1.5 mmol g⁻¹ of OFG and additional 0.3 mmol g⁻¹ of H₂O content in the char material, resulting in an oxygen content of 3.6wt%. However, acid groups are the most important type of OFG when focusing on the influence on adsorption. As the formation of H₂O clusters elucidates, these groups interact strongly with polar adsorbates. The total amount of carboxylic acids in the as-synthesized char results from twice the amount of condensed acids in addition to the amount of acids detected directly.

Table 2 Specific molar amounts n_s of H₂O and individual OFG in the MCC-HTC char sample along with the temperature at the peak of detection

Evolving gas	T [°C]	H ₂ O/OFG	n_s [mmol g ⁻¹]
H ₂ O	150	Physisorption	0.003
H ₂ O	300	Clusters	0.130
H ₂ O	450	Condensation	0.152
CO ₂	220	Condensed acids	0.075
CO	310		
CO ₂	310	Carboxylic acids	0.035
CO ₂	450	Anhydrides	0.086
CO	460		
CO ₂	650	Lactones	0.102
CO	620	Phenols/ethers	0.552
CO	800	Carbonyls/quinones	0.696

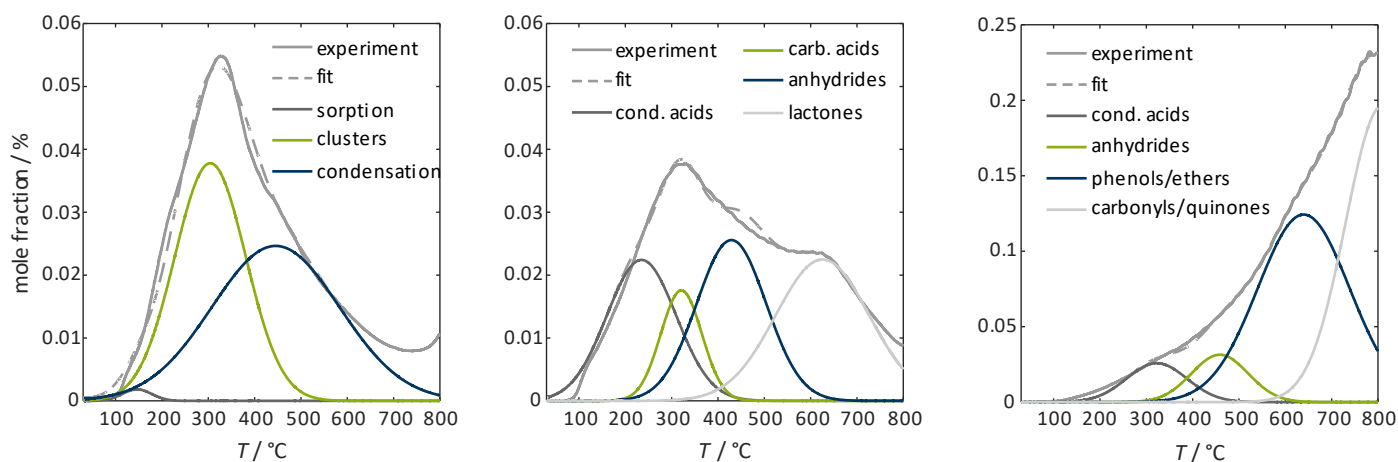


Fig. 2 Effluent gas curves of H_2O (left), CO_2 (center), and CO (right)

Thus, the MCC-HTC char contains about 0.2 mmol g^{-1} of these OFG with a strong potential to interact with adsorbates. Due to the comparatively low quantity of the relevant OFG, the effect of PSD on the shape of the adsorption isotherm and kinetics are expected to prevail.

4.2 Adsorption equilibria

Figure 3 shows exemplarily the experimental results for the adsorption isotherm at $T_{\text{ads}} = 25.4 \text{ }^\circ\text{C}$. For the two points at the lower p/p_{sat} end, a solid-vapor equilibrium at $T_{\text{vapor}} = -10.2 \text{ }^\circ\text{C}$ and $-2.3 \text{ }^\circ\text{C}$ was established to get closer to the lower end of possible H_2O vapor concentration in the measuring cell. For the molecular equilibrium loadings 0.22 mmol/g and 0.42 mmol/g , respectively, no proper kinetics could be recorded.

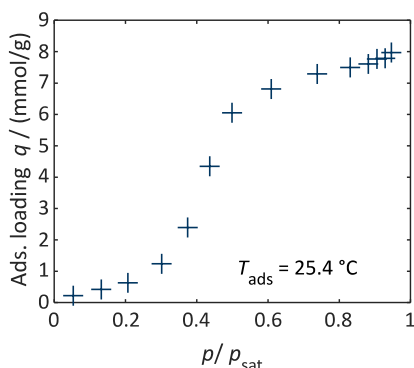


Fig. 3 H_2O adsorption isotherm ($T_{\text{ads}} = 25.4 \text{ }^\circ\text{C}$)

Considering a low concentration of OFG on the surface of the MCC-HTC char particles the adsorption behavior can be ascribed predominantly to the pore structure. Liu et al. [6] reported, that H_2O vapor adsorption in the lower pressure region is initialized by ultramicropores, which provide a deep dispersion potential for H_2O molecules, as described by Striolo et al. [19] The steep increase in the adsorption

loadings for higher pressures is caused by the growth and coalescence of stable H_2O clusters in micropores, developing bridges between each other with thermodynamically favourable concave interfaces. [20] The isotherm in Figure 3 can be characterized as type V [13], which is, considering the ultra-/microporous structure of the investigated MCC-HTC char sample (see Table 1), in good agreement with adsorption data of Nakamura et al. [21] for hydrophobic carbons at a comparable adsorption temperature and similar dominance of ultra-/micropore surfaces.

With respect to a further development of the PSK model, the formulation of the equilibrium part needs to be rethought as the adsorption characteristic is not consistent with the Langmuir approach. From the literature, many models are known to describe the adsorption behavior of H_2O on carbonaceous solids with respect to the different peculiarities of the H_2O adsorption system, e.g. OFG concentrations, variations of cluster sizes or surface heterogeneity. Different model approaches (e.g. by Dubinin and Serpinsky (DS) [22], Do and Do (DD) [23]) and their modifications are assumed to be applicable.

4.3 Adsorption kinetics

The adsorption kinetics are plotted from low (see Figure 4) to high pressures (see Figure 5). It becomes clear that kinetics become systematically slower at higher pressures, but faster again close to saturation. Ito et al. [24] reported the same kinetic behavior for H_2O vapor adsorption on activated carbon with type V isotherm characteristics. They argued that the formation of larger H_2O assemblies and clusters, partially filling micropores, can slow down the adsorption process.

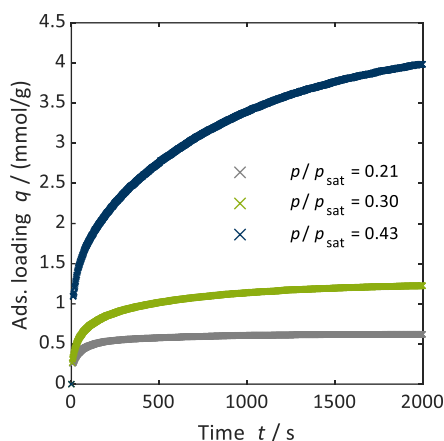


Fig. 4 Adsorption kinetics at low relative pressures and $T_{ads} = 25.4 \text{ } ^\circ\text{C}$

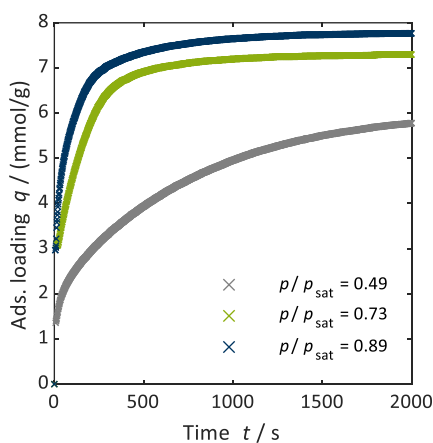


Fig. 5 Adsorption kinetics at high relative pressures and $T_{ads} = 25.4 \text{ } ^\circ\text{C}$

A comprehensive study of the influence of OFG on H₂O vapor adsorption kinetics by Fletcher et al. [7] confirms this behavior. Considering a low presence of OFG on high-temperature treated carbons, decreasing rate constants at higher p/p_{sat} indicate a dominance of associative adsorption over surface functional groups.

As a consequence, the modeling of the kinetic adsorption behavior with respect to the PSK model needs to be rethought. The occurrence of slow and fast kinetics for H₂O vapor is not only necessarily coupled to the morphology-dependent diffusion of molecules through the char particles, but more to the presence, initial formation and diffusion of greater H₂O assemblies.

5. CONCLUSION

In this work the adsorption behavior of H₂O vapor on the MCC-HTC char was investigated in order to establish an experimental data basis for PSK modeling. Therefore, kinetic adsorption measurements were performed along three adsorption isotherms at $T_{ads} = (25.4, 35.3, 48.8) \text{ } ^\circ\text{C}$. Furthermore, the quantification of OFG by TPD

measurements and analysis could be associated to the adsorptive behavior of H₂O vapor. The analysis of the effluent gas curves results in a low content of acid groups (0.2 mmol/g) with respect to the overall amount of OFG (1.5 mmol/g). Due to the low presence of acid groups, the shape of the measured adsorption isotherm is predominantly determined by pore morphology and the formation of H₂O clusters. In the further development of the PSK model, the equilibrium part needs to be modified in consideration of established model approaches for H₂O vapor adsorption, which can be found in the literature.

As part of future research, the kinetic adsorption behavior of H₂O vapor is investigated for other samples e.g. chars from different biomass origin or with an intended higher content of OFG.

ACKNOWLEDGEMENT

Funded by the Deutsche Forschungsgemeinschaft (DFG, German Research Foundation) –Project-ID 215035359–TRR 129 Oxyflame. "Gefördert durch die Deutsche Forschungsgemeinschaft (DFG) –Projektnummer 215035359–TRR 129".

REFERENCE

- [1] Kajitani S, Suzuki N, Ashizawa M, Hara S. CO gasification rate analysis of coal char in entrained flow coal gasifier. *Fuel* 2006;85(2):163–9
- [2] Phounglamcheik A, Bäckebö M, Robinson R, Umeki K. The significance of intraparticle and interparticle diffusion during CO₂ gasification of biomass char in a packed bed. *Fuel* 2022;310:122302
- [3] Wedler C, Richter M, Span R. Integration of sorption kinetics in carbon conversion modeling for the description of oxyfuel combustion processes. *Energy Procedia* 2017;142:1361–6
- [4] Wedler C, Span R. A pore-structure dependent kinetic adsorption model for consideration in char conversion – Adsorption kinetics of CO₂ on biomass chars. *Chemical Engineering Science* 2021;231:116281
- [5] Wedler C, Eisenbach T, Schwarz J, Span R. A first parameterization of the pore-structure dependent kinetic adsorption model for O₂ adsorption in biomass conversion modeling. In: *ICAE 2021 Proceedings*; 2021
- [6] Liu L, Tan SJ, Horikawa T, Do DD, Nicholson D, Liu J. Water adsorption on carbon - A review. *Advances in colloid and interface science* 2017;250:64–78
- [7] Fletcher AJ, Uygur Y, Thomas KM. Role of Surface Functional Groups in the Adsorption Kinetics of Water

Vapor on Microporous Activated Carbons. *J. Phys. Chem. C* 2007;111(23):8349–59

[8] Boehm HP. Some aspects of the surface chemistry of carbon blacks and other carbons. *Carbon* 1994;32(5):759–69

[9] Pflieger C, Wedler C, Eckhard T, Schulwitz J, Eisenbach T, Ontyd C et al. The Influence of Conversion in Diluted O₂ and CO₂ on Textural, Structural, and Chemical Properties in Correlation to the Reactivity of Cellulose-Derived Chars. to be submitted

[10] Lotz K, Wütscher A, Düdler H, Berger CM, Russo C, Mukherjee K et al. Tuning the Properties of Iron-Doped Porous Graphitic Carbon Synthesized by Hydrothermal Carbonization of Cellulose and Subsequent Pyrolysis. *ACS omega* 2019;4(2):4448–60

[11] Wedler C, Lotz K, Arami-Niya A, Xiao G, Span R, Muhler M et al. Influence of Mineral Composition of Chars Derived by Hydrothermal Carbonization on Sorption Behavior of CO₂, CH₄, and O₂. *ACS omega* 2020;5(19):10704–14

[12] Jagiello J, Kenvin J, Celzard A, Fierro V. Enhanced resolution of ultra micropore size determination of biochars and activated carbons by dual gas analysis using N₂ and CO₂ with 2D-NLDFT adsorption models. *Carbon* 2019;144:206–15

[13] Thommes M, Kaneko K, Neimark AV, Olivier JP, Rodriguez-Reinoso F, Rouquerol J et al. Physisorption of gases, with special reference to the evaluation of surface area and pore size distribution (IUPAC Technical Report). *Pure and Applied Chemistry* 2015;87(9-10):1051–69

[14] Figueiredo JL, Pereira MFR, Freitas MMA, Órfão JMM. Characterization of Active Sites on Carbon Catalysts. *Ind. Eng. Chem. Res.* 2007;46(12):4110–5

[15] Ortega KF, Arrigo R, Frank B, Schlögl R, Trunschke A. Acid–Base Properties of N-Doped Carbon Nanotubes: A Combined Temperature-Programmed Desorption, X-ray Photoelectron Spectroscopy, and 2-Propanol Reaction Investigation. *Chem. Mater.* 2016;28(19):6826–39

[16] Rösler M, Wedler C. Adsorption kinetics and equilibria of two methanol samples with different water content on activated carbon. *Adsorption* 2021;27(8):1175–90

[17] Wagner W, Pruss A. International Equations for the Saturation Properties of Ordinary Water Substance. Revised According to the International Temperature Scale of 1990. Addendum to *J. Phys. Chem. Ref. Data* 16 893 (1987). *Journal of Physical and Chemical Reference Data* 1993;22(3):783–7

[18] Boehm H. Surface oxides on carbon and their analysis: a critical assessment. *Carbon* 2002;40(2):145–9

[19] Striolo A, Chialvo AA, Cummings PT, Gubbins KE. Water Adsorption in Carbon-Slit Nanopores. *Langmuir* 2003;19(20):8583–91

[20] Horikawa T, Muguruma T, Do DD, Sotowa K, Alcántara-Avila JR. Scanning curves of water adsorption on graphitized thermal carbon black and ordered mesoporous carbon. *Carbon* 2015;95:137–43

[21] Nakamura M, Ohba T, Branton P, Kanoh H, Kaneko K. Equilibration-time and pore-width dependent hysteresis of water adsorption isotherm on hydrophobic microporous carbons. *Carbon* 2010;48(1):305–8

[22] Dubinin M, Serpinsky V. Isotherm equation for water vapor adsorption by microporous carbonaceous adsorbents. *Carbon* 1981;19(5):402–3

[23] Do DD, Junpirom S, Do HD. A new adsorption–desorption model for water adsorption in activated carbon. *Carbon* 2009;47(6):1466–73

[24] Ito H, Iiyama T, Ozeki S. Kinetics of Cluster-Mediated Filling of Water Molecules into Carbon Micropores. *J. Phys. Chem. C* 2015;119(8):4118–25